

**What controls springtime fine dust variability in the western United States?
Investigating the 2002-2015 increase in fine dust in the U.S. Southwest**

Pattanun Achakulwisut¹, Lu Shen², and Loretta J. Mickley²

¹Department of Earth and Planetary Sciences, Harvard University, Cambridge, MA, USA

²School of Engineering and Applied Sciences, Harvard University, Cambridge, MA, USA

Contents of this file

Text S1 to S5

Figures S1 to S12

Table S1

Introduction

This supporting information provides additional figures and tables, and further discussions related to the data processing and results validation methods.

Text S1. Deriving monthly mean fine dust concentrations from PM_{2.5}-Iron

The IMPROVE network consists of automated samplers that collect PM₁₀ (aerodynamic diameter less than 10 µm) and PM_{2.5} aerosol fractions on filters for a 24-hour period every third day. Only the PM_{2.5} filters are routinely analyzed for chemical composition (*Malm et al.*, 2004). Total dust concentration is commonly defined as the sum of the concentrations of coarse mass (i.e., [PM₁₀] – [PM_{2.5}]) and the soil-derived component of PM_{2.5} (e.g., *Wells et al.*, 2007; *Kavouras et al.*, 2007, 2009). This definition assumes that all coarse mass is dust. In this study, we choose to focus on just the fine fraction of mineral dust for four reasons: (1) observations at a subset of IMPROVE sites show that carbonaceous material and inorganic salts may contribute up to 50% of the coarse mass fraction (*Malm et al.*, 2007); (2) the magnitude of coarse mass concentrations is almost always much higher (by 5-10 times) than that of fine dust, swamping potential trends in fine dust; (3) fine dust has a longer atmospheric lifetime than coarse dust, giving it a greater capacity for long-distance transport and regional-scale impacts; and (4) fine particles are primarily responsible for visibility reduction (*Malm*, 1999), and particles less than 1 µm in size are known to have the most adverse effects on human health, as they can penetrate deep into the lungs (e.g., *Kim et al.*, 2015).

Fine mineral dust is commonly reconstructed from the mass concentrations of soil-derived elements and their normal oxides, along with a correction factor to account for other species such as water and carbonate. For example, the operation definition of “Fine Soil” in the IMPROVE network is (*Malm et al.*, 1994, 2004):

$$[\text{Fine soil}] = 2.2 \times [\text{Al}] + 2.49 \times [\text{Si}] + 1.63 \times [\text{Ca}] + 2.42 \times [\text{Fe}] + 1.94 \times [\text{Ti}]. \quad (\text{S1})$$

The speciated-PM_{2.5} measurements by the IMPROVE network includes Al, Si, Ca, Fe, and Ti. However, in their analysis of archived IMPROVE aerosol samples from 1995-2010, *Hyslop et al.* (2015) found that out of the five elements commonly used to define Fine Soil (Eqn. S1), only iron and calcium provide reliable time series at sites where these elements have been measured above their respective detection limits for more than 80% of the time period considered. Changes in analytical methods over time have introduced spurious trends in silicon, titanium, and aluminum. Since 2011, a new Panalytical XRF system has been used to determine elemental concentrations at all IMPROVE sites (*Hand et al.*, 2017). *Hand et al.* (2016) approximated fine dust as 3.5% Fe,

based on the average elemental composition of the upper continental crust (*Taylor and McLennan, 1985; McLennan, 2001*).

Instead of using the IMPROVE operational Fine Soil definition (Eqn. 1), we follow the approach of Hand et al. (2016) in using the iron content of filter samples as a fine dust proxy with some modifications. We calculate monthly mean fine dust concentrations as follows: (1) We neglect any sites at which PM_{2.5}-Iron is measured below the minimum detection limit for more than 20% of the total measurements available during the 14-year period. (2) We screen out “high-combustion” days when the elemental carbon (EC) concentration exceeds a threshold value, defined as the 2002-2015 EC monthly mean + 1 standard deviation for a given site (~12% of data removed in total). (3) For each site and month containing at least 50% complete data, we calculate monthly mean PM_{2.5}-Iron concentrations from daily values. (4) We approximate monthly mean fine dust concentrations as PM_{2.5}-Iron/0.058.

We include step (2) because *Wang et al. (2015)* estimated that atmospheric iron emissions are primarily due to mineral sources in the Southwest, whereas combustion sources (fossil fuels, biofuels, and biomass) may also contribute in the Northwest and California. We find that the 2002-2015 trends in monthly mean fine dust concentration across the western United States are not sensitive to the threshold EC value in step (2), as discussed below in Section S3.

In Step (4), we approximate fine dust as PM_{2.5}-Iron/0.058 based on the observed linear relationships between daily PM_{2.5}-Iron and Fine Soil from 2011 to 2015 for the 91 IMPROVE sites included in this study (Figure S1). *Lawrence and Neff (2009)* demonstrated that on average globally, the concentrations of most major elements (Si, Al, Fe, Mg, Ca, K) in aeolian dust tend to be similar to the composition of the upper continental crust. For Iron, the observed mean value is 3.6% (range of 1.3-7.8%). Our derived value of 5.8% is consistent with these estimates. We also check that the linear correlation between PM_{2.5}-Iron and Fine Soil applies to each site. For the 91 sites selected in this study, the correlation coefficients are all greater than 0.91 ($p < 0.05$). Converting PM_{2.5}-Iron to fine dust by site-specific scaling factors (ranging from 0.050-0.093) yield similar EOF results in terms of the spatiotemporal variability observed for each spring month (not shown).

Text S2. Monthly mean fine dust vs. frequency of extreme dust events

IMPROVE measurements are made on average every third day. Given that in the Southwest, dust storms frequently occur in the spring months but rarely exceed 24 hours in duration, the calculated

monthly mean fine dust concentrations may be biased high or low relative to the true value for different months. To check whether the calculated monthly mean concentrations may be representative of the frequency of extreme dust events, we calculate the 2002-2015 MAM monthly frequency of fine dust event days (FDEDs) as follows. (1) For each site and month, we calculate the total number of days N with measurements. (2) We next determine the number of days $nFDED$ for which the daily fine dust concentration exceeds a threshold value, defined as the 2002-2015 monthly mean + 1 standard deviation for a given site and month. (3) We calculate the monthly frequency of dust event days as $nFDED*100/N$.

Figure S2 shows the time series of 2002-2015 monthly mean fine dust concentrations versus monthly FDED frequency averaged over four different domains across the western United States. The domains are “Northwest” (40°-49°N, 111°-125°W), “Southern California” (31°-39°N, 116°-122°W), “Northern Rockies & Plains” (41°-49°N, 100°-111°W), and “Southwest” (31°-39°N, 100°-115°W). For all regions and months, the two time series are significantly correlated ($p < 0.05$) with correlation coefficients ranging from 0.87-0.99. These results suggest that the monthly mean fine dust concentrations are also representative of the frequency of extreme dust events, at least with respect to the $PM_{2.5}$ fraction.

In addition, Tong et al. (2017) used cluster analysis to construct a time series of dust storm frequency from IMPROVE measurements in the southwestern United States between 1998-2011. They also found negative correlations between dust storm frequency and PDO and ENSO for all months, which is consistent with our results.

Text S3. Definition of “high-combustion” day

In calculating the monthly mean fine dust concentration based on $PM_{2.5}$ -Iron concentrations, we screen out “high-combustion” days when the elemental carbon (EC) concentration exceeds a threshold value, defined as the 2002-2015 monthly mean + 1 standard deviation for a given site. In this section, we explore the sensitivity of the 2002-2015 springtime trends in fine dust concentrations in the western United States to a range of EC threshold values: 95th, 85th, and 75th percentile of 2002-2015 daily EC concentrations for a given site. The 85th percentile threshold value is comparable to our metric of mean + 1 standard deviation.

As shown in Figure S3, the 2002-2015 March trends in monthly mean fine dust concentration across the western United States appear to be relatively insensitive to the EC

threshold value. This finding also applies to April and May (not shown). As in Figure 1, Figures S3a-c display a strong north-south contrast in which most sites located below 40°N across the West display increasing statistically significant trends in March over the 14-year period, whereas sites above 40°N do not.

Text S4. EOF analysis results using PM_{2.5}-Calcium as a fine dust proxy

We also calculate monthly mean fine dust concentrations using PM_{2.5}-Calcium as a proxy, following the method outlined in section S1 for PM_{2.5}-Iron, but assume fine dust to be 8.4% PM_{2.5}-Calcium (Figure S1). We then repeat the EOF analysis outlined in section 2.4. The first two EOF modes for each of the spring months have spatiotemporal patterns consistent with those derived from PM_{2.5}-Iron-based fine dust: 50-65% of the fine dust interannual variability in each spring month is captured by the first two leading modes, which consist of a uniform co-variability across almost all sites in the western United States and a Northwest-Southwest dipole of variability (Figure S9). The only difference is that the dominance of the uniform versus the Northwest-Southwest dipole pattern of co-variability is switched for March.

Text S5. Validating assumptions and assessing predictive power of Multiple Linear Regression models

For each of the regression models, we validate four key assumptions of multiple linear regression analysis:

1. **Linearity:** This assumption assumes that the true relationship between the dependent variable and the independent variables are linear. We examine this using X-Y scatterplots. Although the EOF-correlation analyses suggest that surface mean/maximum temperature also influences fine dust variability, we find that the linear correlations between regional mean fine dust and temperature are weak ($r < 0.3$). Given that a key assumption of MLR is that the true relationship between the dependent and independent variables are linear, we exclude surface temperature from the list of potential predictors. At least on a regional scale, the influence of temperature on fine dust appears to be mainly exerted through its contribution to determining the land surface water balance.

2. Homoscedasticity: This assumption requires that the error between observed and predicted values (i.e., the regression residuals) is the same across all values of the independent variable. We test this by plotting the standardized residuals against the predicted values.
3. Normality of errors: This assumption requires that the error between observed and predicted values (i.e., the regression residuals) should be normally distributed. We test this with a Q-Q plot.
4. Multicollinearity: This assumption assumes that the independent variables are not highly correlated with each other. We test this by checking that the Variance Inflation Factor (VIF) of the selected parameters does not exceed a value of 10. VIF is defined as $1/(1 - R_k^2)$, where R_k^2 is the coefficient of multiple determination obtained by regressing the k^{th} predictor on the remaining parameters.

We also extend the modeled values back to 1990 and compare it to available observations for 1990-2011 (Figures S11-S12). The correlation coefficient between 1990-2001 observed and predicted values is 0.56 ($p = 0.07$) for the Pacific Southwest domain and 0.68 ($p = 0.02$) for the Central Southwest domain.

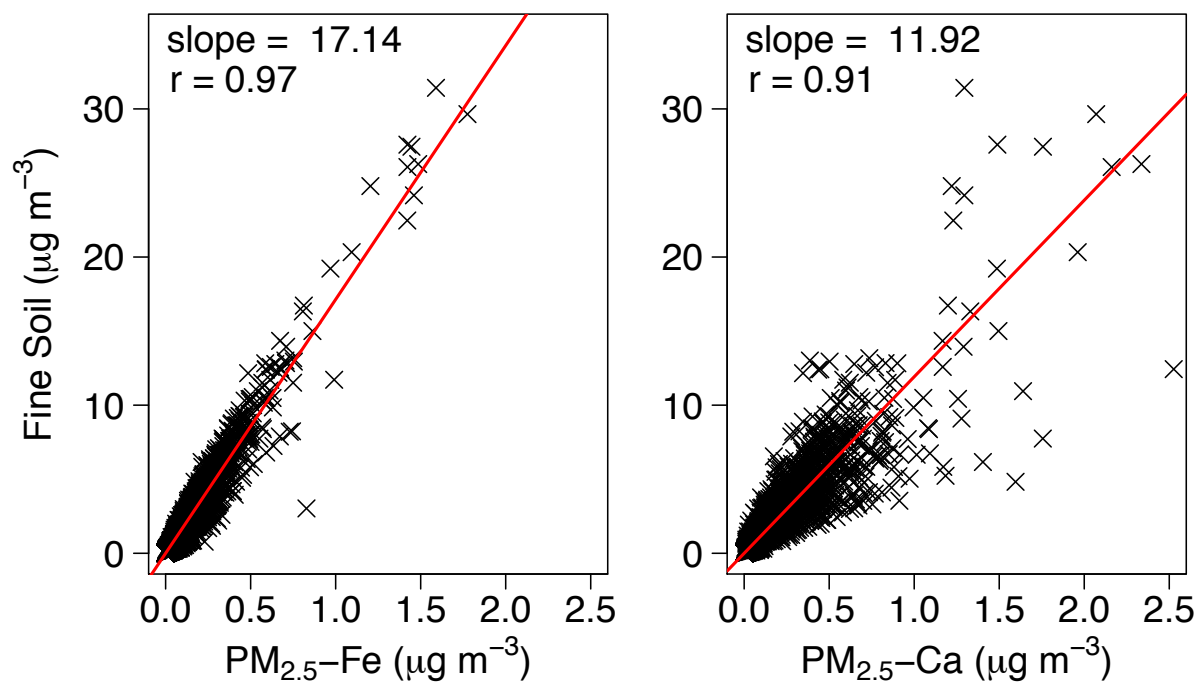


Figure S1. IMPROVE 2011-2015 MAM daily mean Fine Soil vs. PM_{2.5}-Iron (left panel) and Fine Soil vs. PM_{2.5}-Calcium (right panel) concentrations with “high combustion days” screened out across IMPROVE sites located in the western U.S. domain. The red lines show the linear regressions with the intercept fixed at zero. The statistically significant ($p < 0.05$) slope values and correlation coefficients are shown inset.

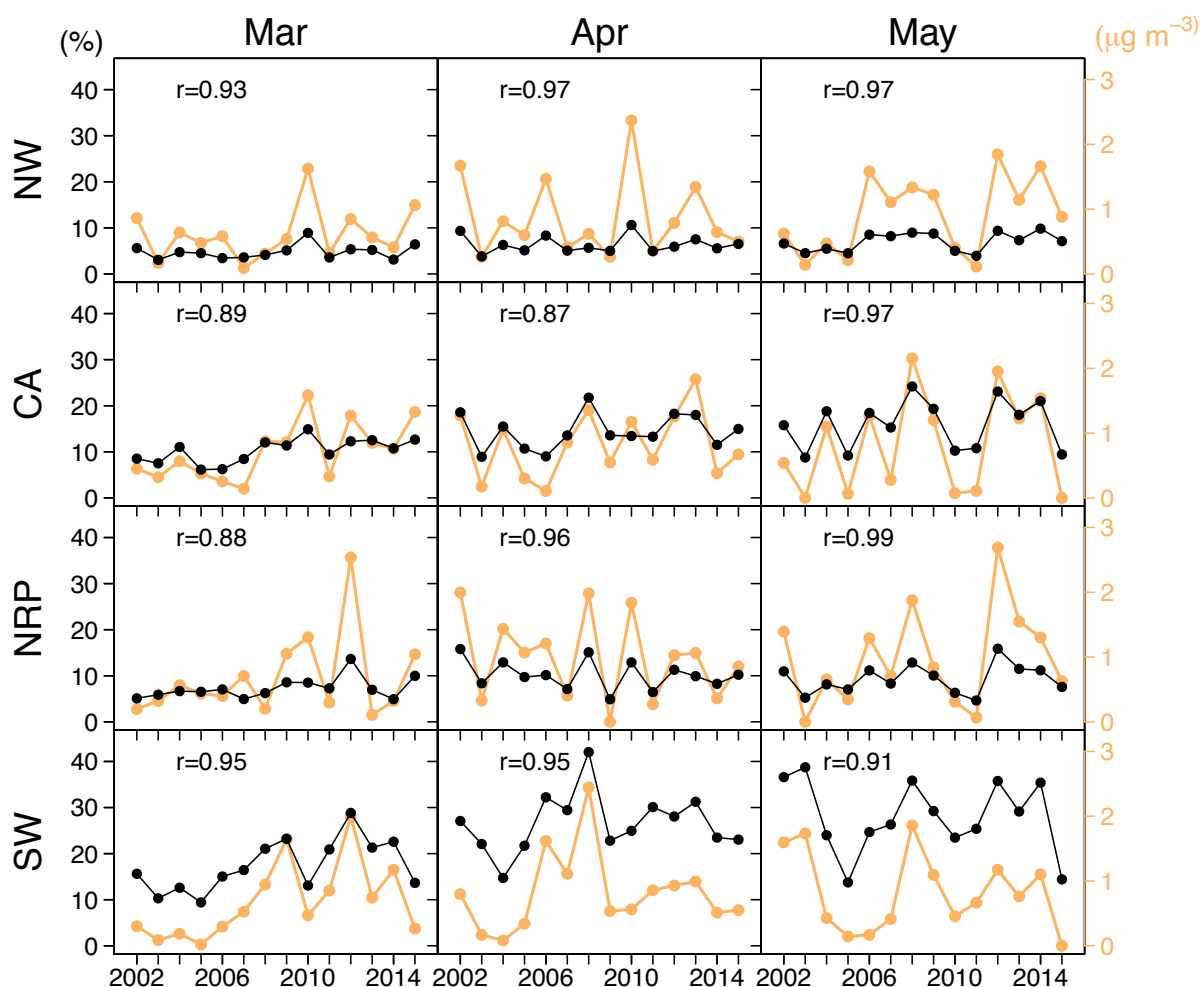


Figure S2. IMPROVE 2002-2015 MAM monthly frequency of “fine dust event days” (FDEDs, black) and monthly mean fine dust concentration (orange) averaged for four different regions across the western United States. The regions are Northwest (“NW”), Southern California (“CA”), Northern Rockies and Plains (“NRP”), and Southwest (“SW”). The statistically significant ($p < 0.05$) correlation coefficients between the two time series for each month and region are shown inset.

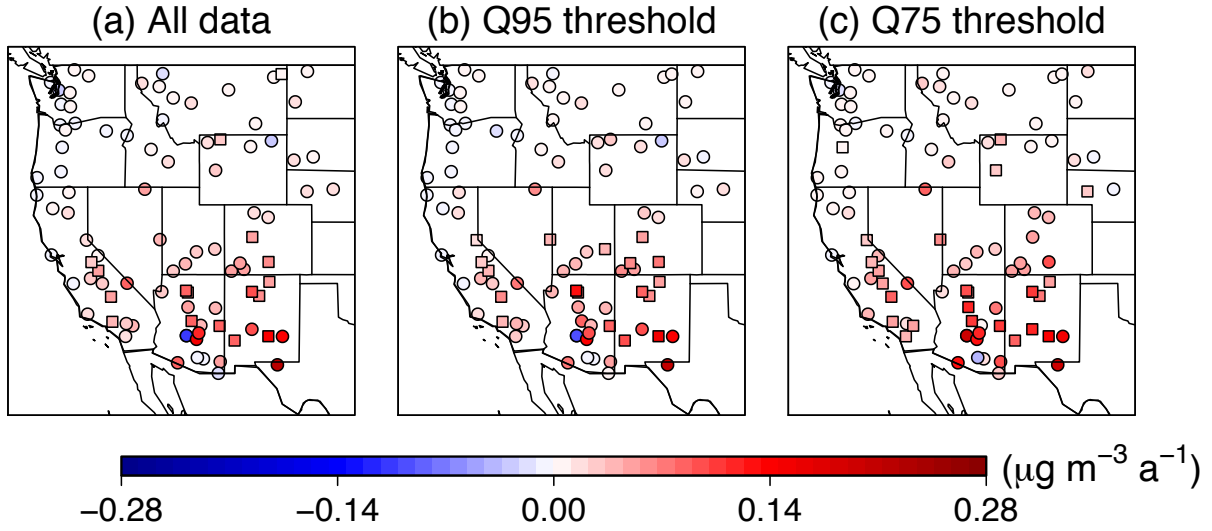


Figure S3. Trends of monthly mean fine dust concentrations from 2002 to 2015 in March at IMPROVE network sites across the western United States (31°-49°N, 100°-125°W). Square symbols denote sites with statistically significant trends ($p < 0.05$). Fine dust is derived from $\text{PM}_{2.5}$ -Iron. Monthly mean concentrations are calculated from daily values with “high-combustion” days screened out, using a range of site-specific elemental carbon (EC) threshold values. In panel (a), no data are excluded. In panels (b)-(c), daily fine dust data are excluded if the EC concentration for a given day and site exceeds the labeled percentile of 2002-2015 daily EC concentrations. The Mann-Kendall test is used to assess the statistical significance of a monotonic trend, and the Theil-Sen estimator is used to calculate the slope of the trend. Only sites with at least 7 years of data over the 14-year period are included.

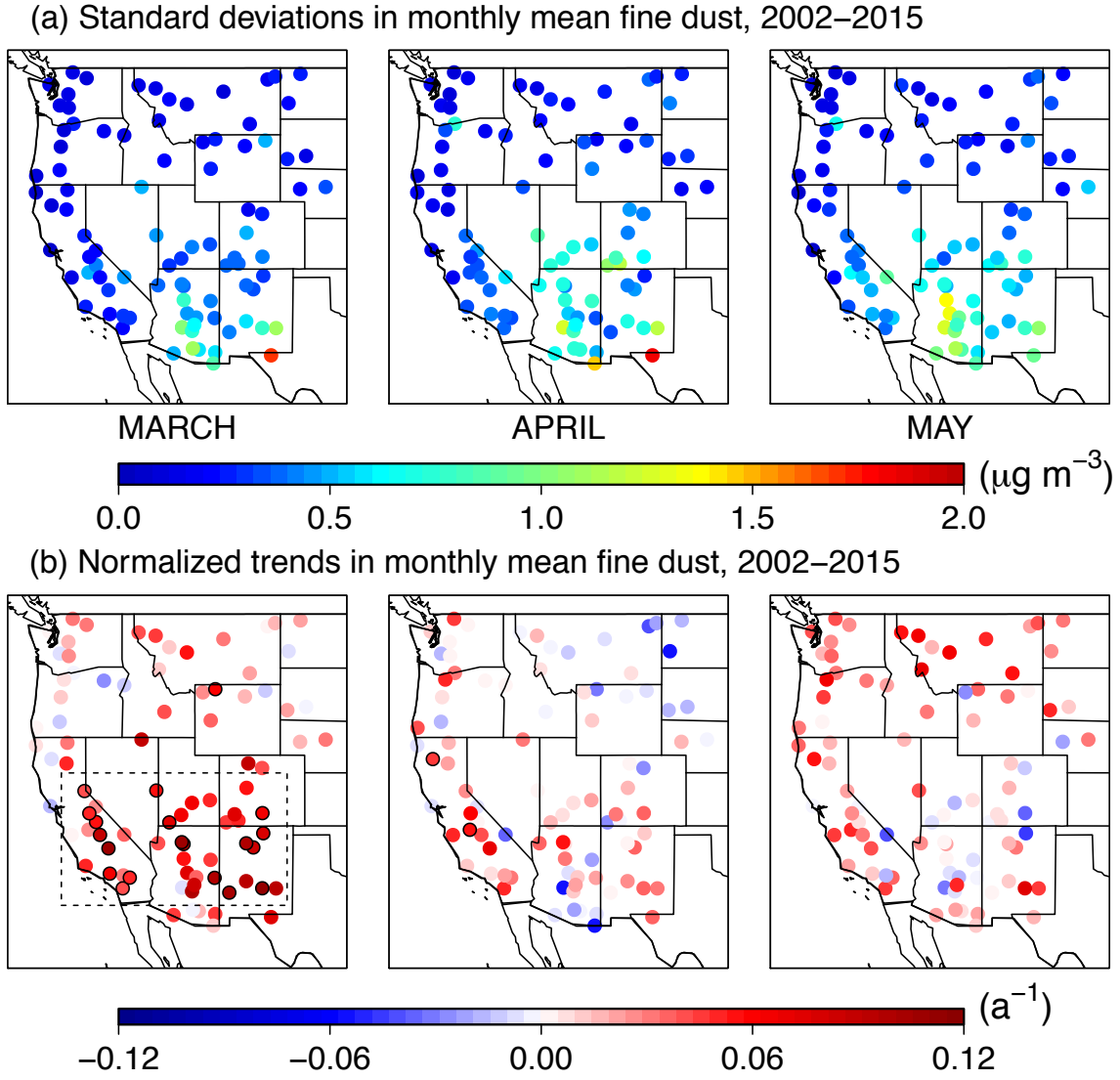


Figure S4. a) Monthly mean standard deviations of fine dust concentrations from 2002 to 2015 March-May at IMPROVE network sites across the western United States (31° - 49° N, 100° - 125° W). b) Normalized trends of monthly mean fine dust concentrations. Trends are normalized by the site-specific 2002-2015 concentrations. Symbols with black outlines denote sites with statistically significant trends ($p < 0.05$). Monthly mean values are calculated from daily values with “high-combustion” days screened out. Only sites with at least 7 years of data over the 14-year period are included.

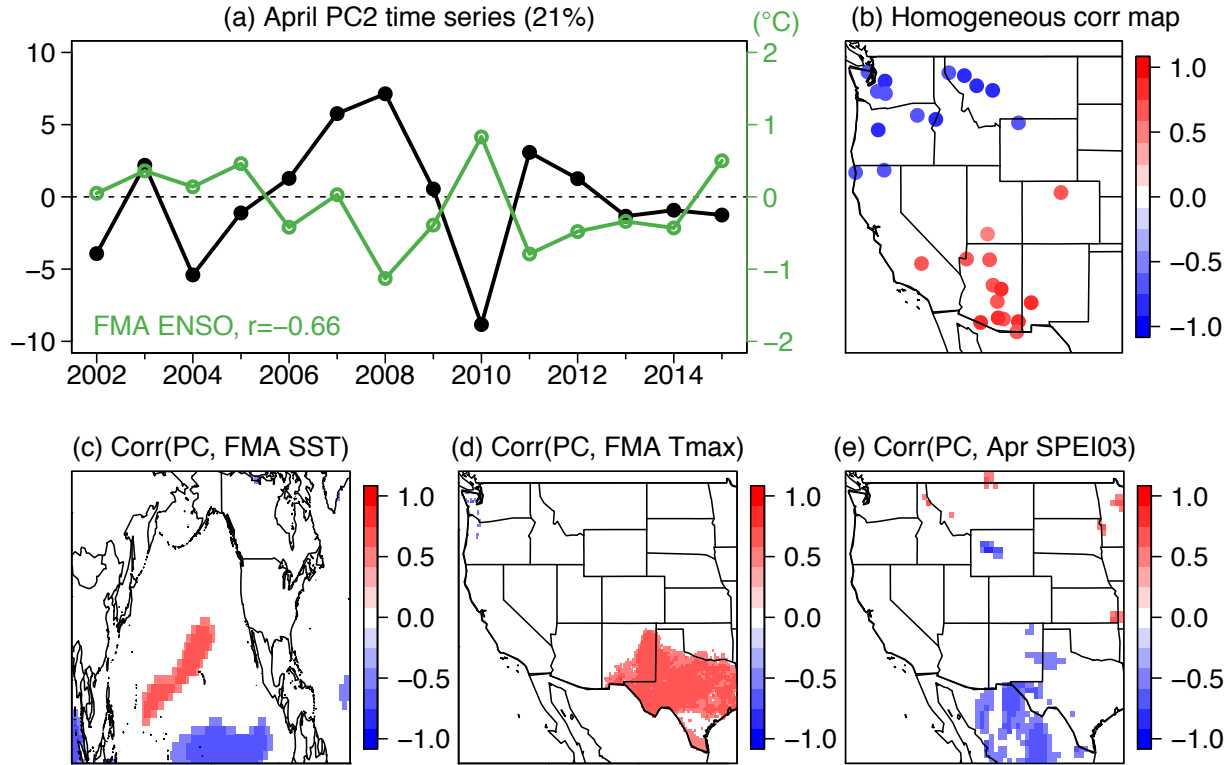


Figure S5. Analysis of the 2nd EOF mode of standardized monthly anomalies of April fine dust concentrations between 2002 and 2015, which explains 21% of the total variance. (a) Time series of the principal components of the 2nd EOF mode (“PC2”). The panel also shows the time series of current-year FMA El Niño-Southern Oscillation (ENSO) ONI index (green). The correlation of the ENSO index with April PC2 is shown inset. The left axis corresponds to PC2 values and the right axis corresponds to the ENSO index. (b) Homogeneous correlation map between PC2 and the time series of standardized monthly fine dust anomalies at IMPROVE sites. The second row panels show heterogeneous correlation maps between PC2 and the time series of current-year FMA (c) sea surface temperatures (SST), (d) maximum surface air temperature (Tmax), and (e) April 3-month Standardized Precipitation-Evapotranspiration Index (SPEI03). In panels (b)-(e), only those sites or grid cells with statistically significant correlations ($p < 0.05$) are shown. Monthly meteorological variables are detrended but not standardized.

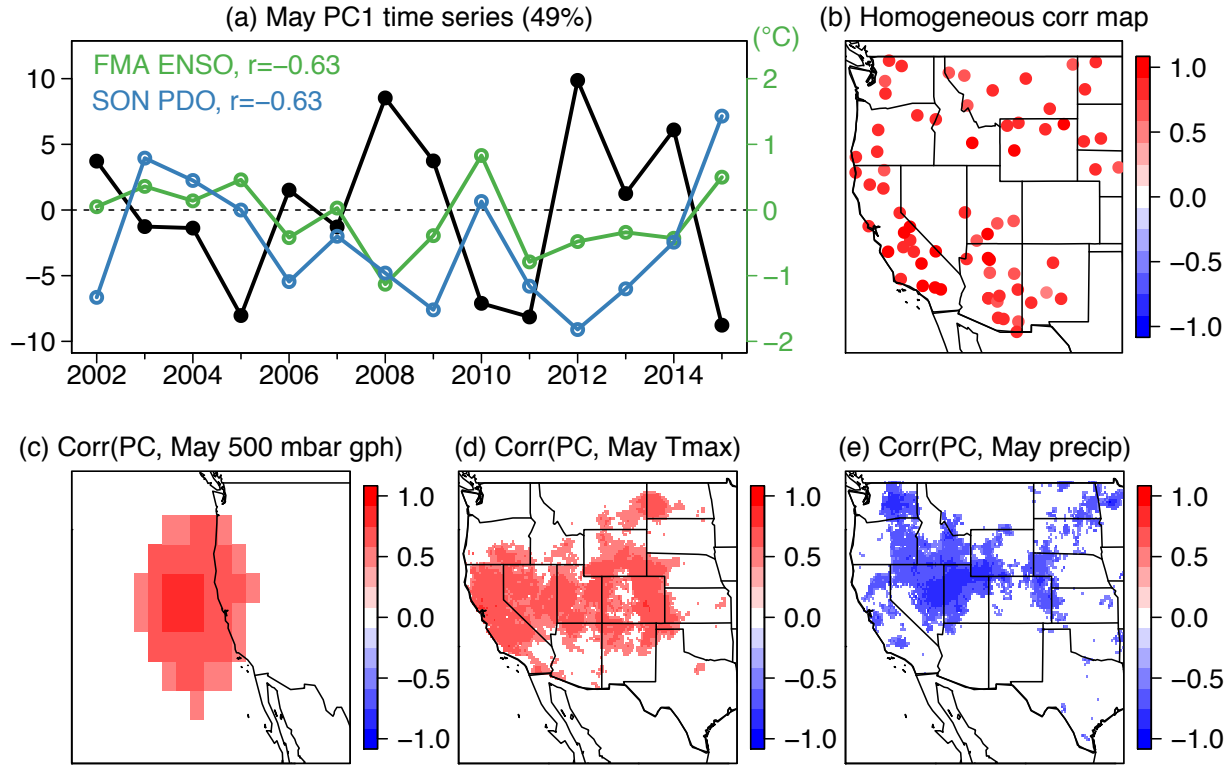


Figure S6. Analysis results of the 1st EOF mode of standardized monthly anomalies of May fine dust concentrations between 2002 and 2015, which explains 49% of the total variance. (a) Time series of the principal components of the 1st EOF mode (“PC1”). The panel also shows the time series of current-year FMA El Niño-Southern Oscillation (ENSO) ONI index (green) and previous-year SON Pacific Decadal Oscillation (PDO) index (blue). Correlations of these indices with March PC1 are shown inset. The left axis corresponds to PC1 values and the right axis corresponds to the ENSO and PDO indices. (ONI values have units of °C whereas PDO values are unitless.) (b) Homogeneous correlation map between PC1 and the time series of standardized monthly fine dust anomalies at IMPROVE sites. The second row panels show heterogeneous correlation maps between PC1 and May (c) 500 mb geopotential height, (d) maximum surface air temperature (Tmax), and (e) total precipitation (rain and snow). In panels (b)-(e), only those sites or grid cells with statistically significant correlations ($p < 0.05$) are shown. Monthly meteorological variables are detrended but not standardized.

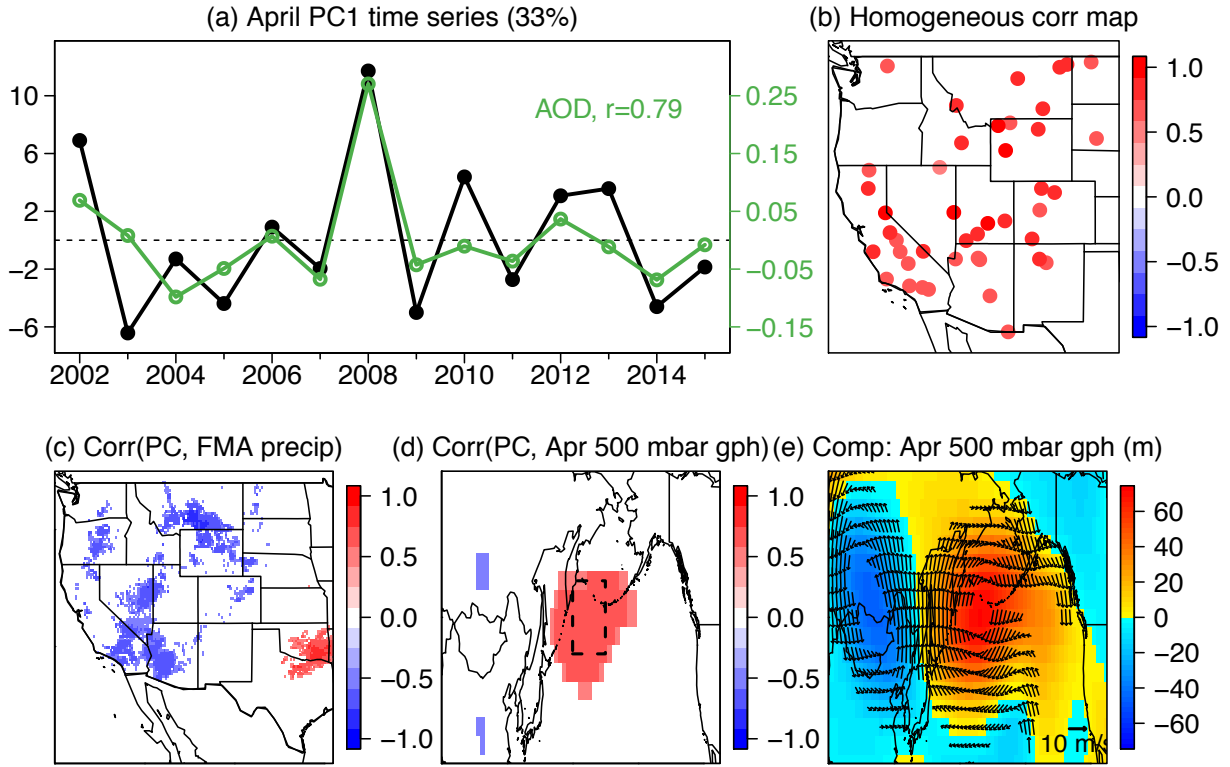


Figure S7. Analysis results of the 1st EOF mode of standardized monthly anomalies of April fine dust concentrations between 2002 and 2015, which explains 33% of the total variance. (a) Time series of the principal components of the 1st EOF mode (“PC1”). The panel also shows the detrended April time series of MODIS 550-nm aerosol optical depth (AOD, green) averaged over 45°-55°N, 160°-180°E (outlined by dashed box in panel d). The correlation between the AOD and PC1 time series is shown inset. (b) Homogeneous correlation map between PC1 and the time series of standardized monthly fine dust anomalies at IMPROVE sites. The second row panels show heterogeneous correlation maps between PC1 and current-year (c) FMA total precipitation (rain and snow), and (d) April 500 mb geopotential height. In (e), composite anomalies associated with positive PC1 years for April 500 mb geopotential height (m) are shown, overlaid by wind field anomalies (only wind speeds $> 2 \text{ m s}^{-1}$ plotted as black arrows). In panels (b)-(d), only those sites or grid cells with statistically significant correlations ($p < 0.05$) are shown. Monthly meteorological variables are detrended but not standardized.

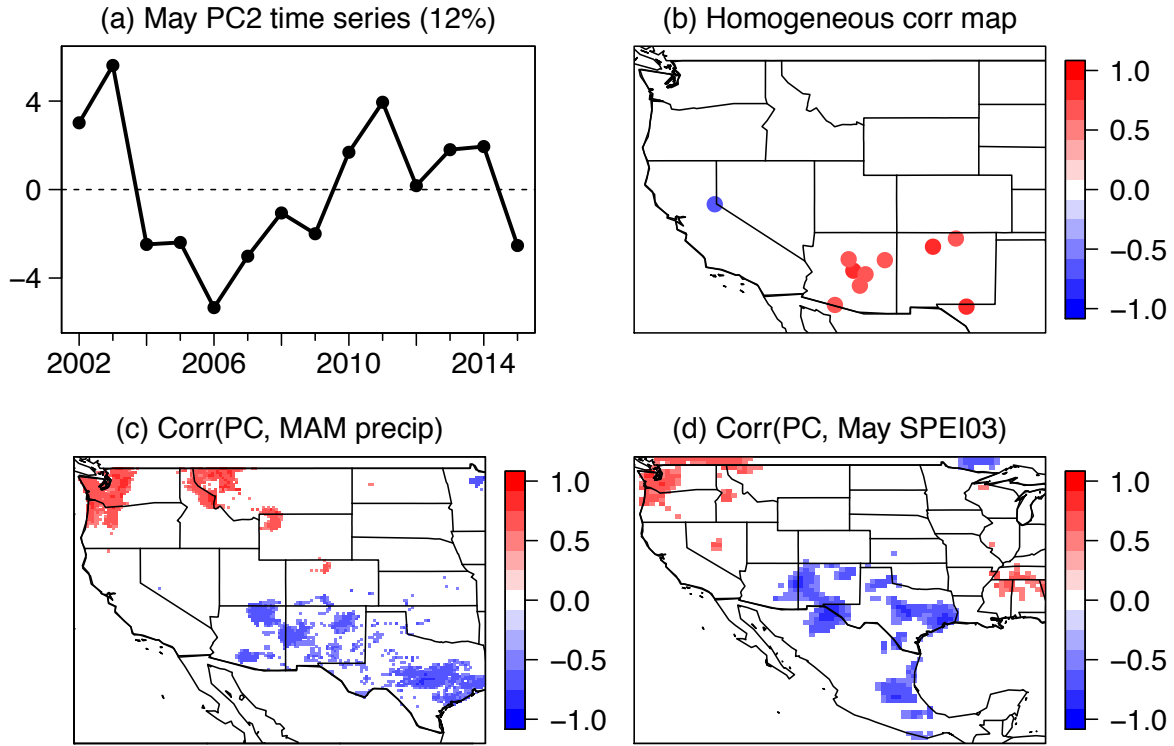
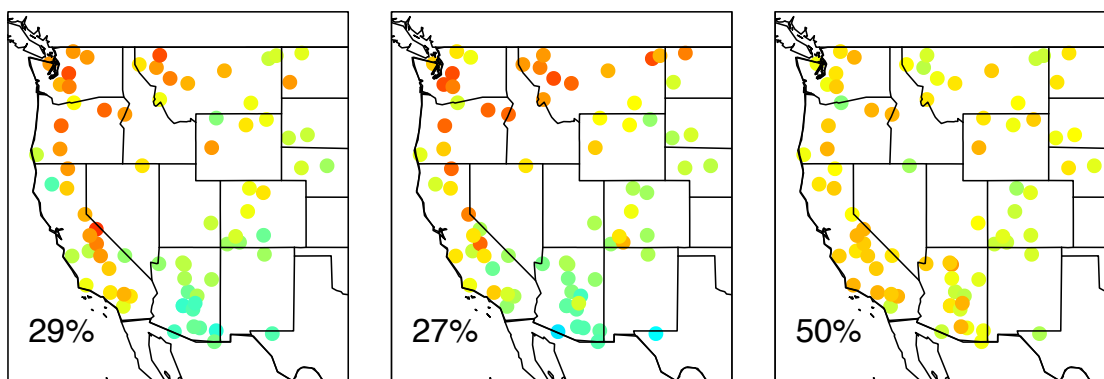
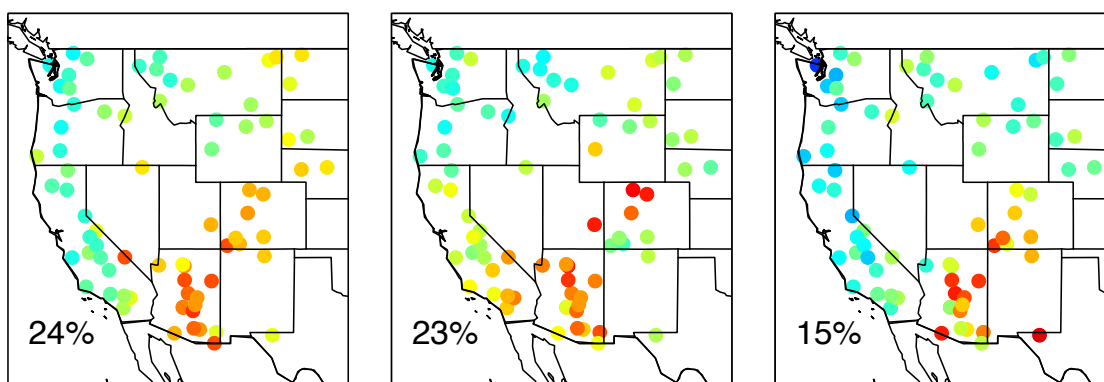


Figure S8. Analysis results of the 2nd EOF mode of standardized monthly anomalies of May fine dust concentrations between 2002 and 2015, which explains 12% of the total variance. (a) Time series of the principal components of the 2nd EOF mode (“PC2”). (b) Homogeneous correlation map between PC2 and the time series of standardized monthly fine dust anomalies at IMPROVE sites. The second row panels show heterogeneous correlation maps between PC2 and current-year (c) MAM total precipitation (rain and snow), and (d) May 3-month Standardized Precipitation-Evapotranspiration Index (SPEI03). In panels (b)-(d), only those sites or grid cells with statistically significant correlations ($p < 0.05$) are shown. Monthly meteorological variables are detrended but not standardized.

(a) 1st EOF loading



(b) 2nd EOF loading



MARCH

APRIL

MAY

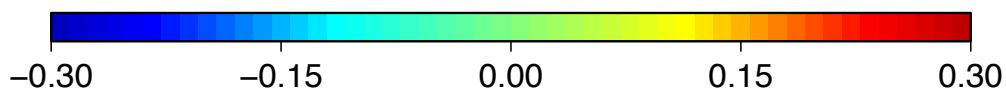


Figure S9. EOF loadings of standardized anomalies of monthly mean fine dust concentrations for 2002-2015 March-May, using $\text{PM}_{2.5}$ -Calcium as a fine dust proxy. For each month, the first EOF mode is shown in the top row and the second EOF mode is shown in the bottom row. The percentage of total variance explained by each EOF mode for a given month is displayed inset.

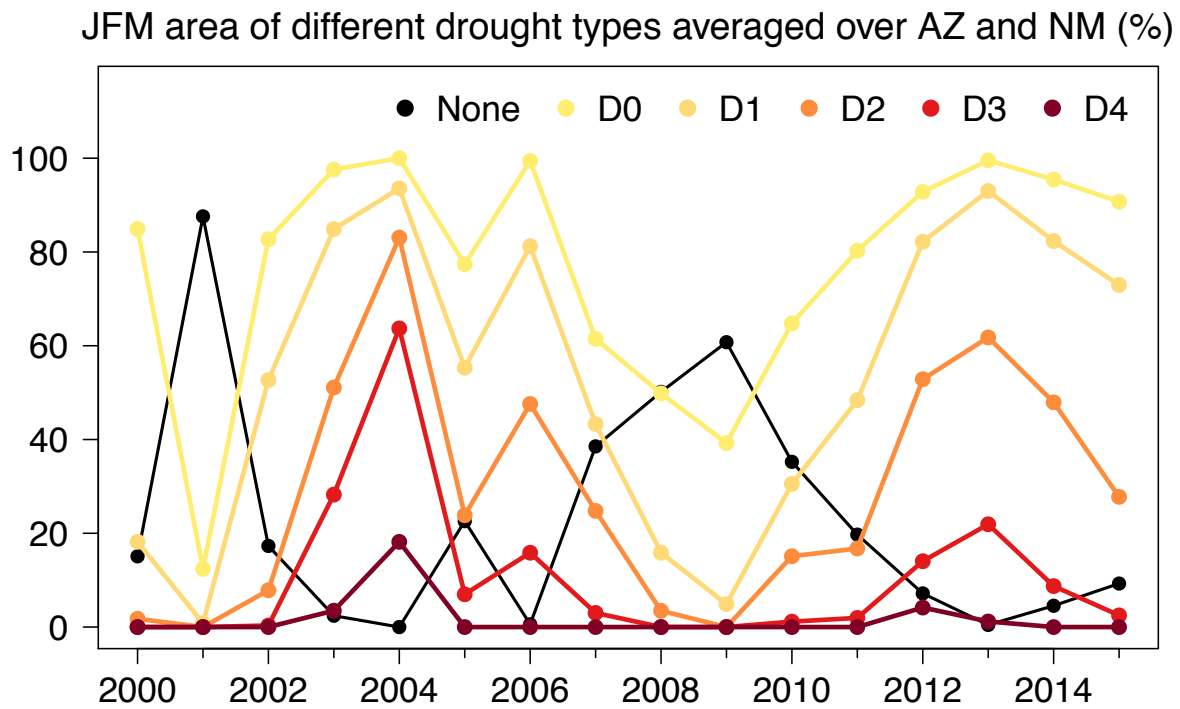


Figure S10. Time series of percent land areas (%) averaged over the states of Arizona and New Mexico experiencing different drought types over 2000-2015 in January-March, with “None” indicating no drought (black) and the different colors denoting drought severity: “D0 Abnormally Dry” (yellow), “D1 Moderate Drought” (light orange), “D2 Severe Drought” (orange), “D3 Extreme Drought” (red) and “D4 Exceptional Drought” (dark red). Data are from the National Drought Mitigation Center (<http://droughtmonitor.unl.edu/MapsAndData/Graph.aspx>).

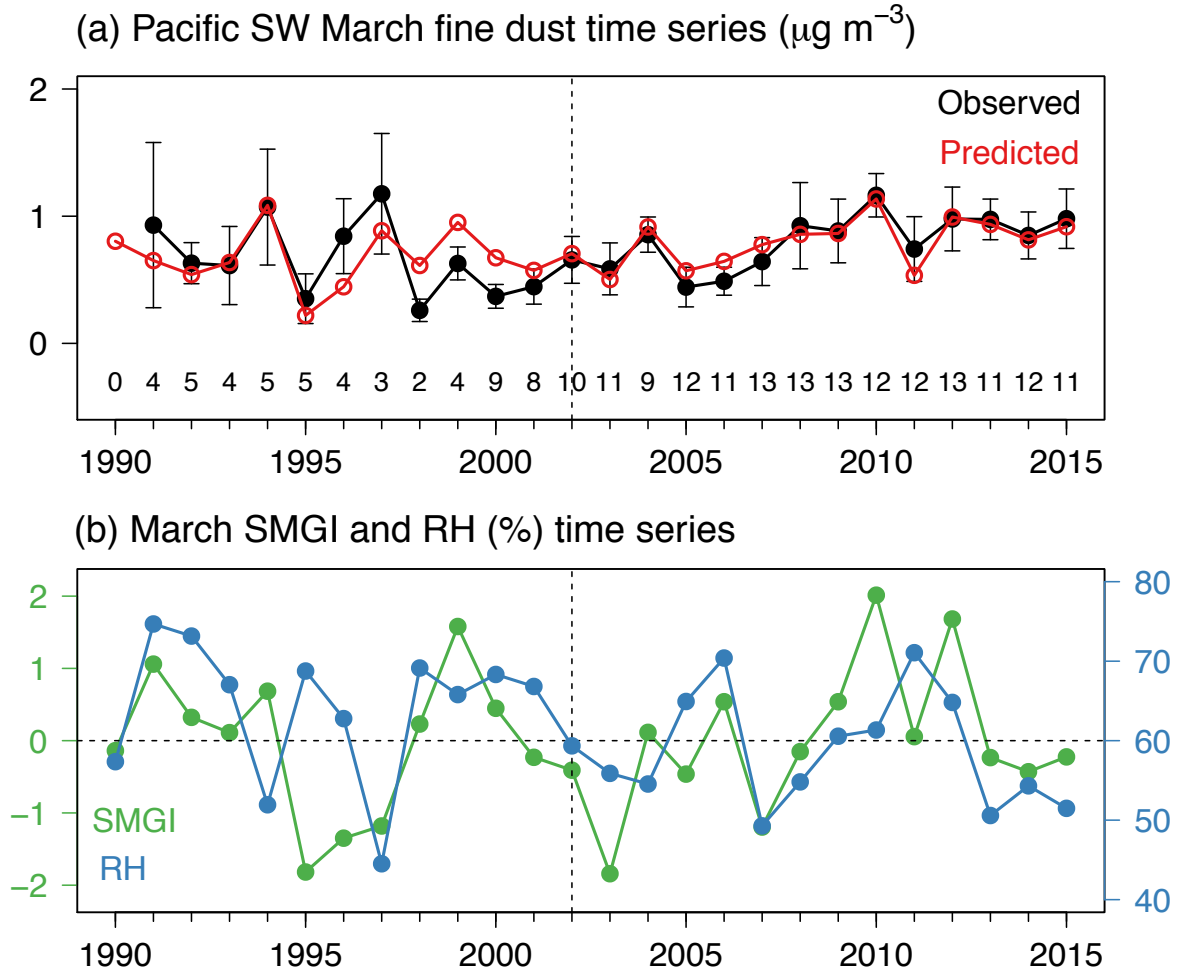
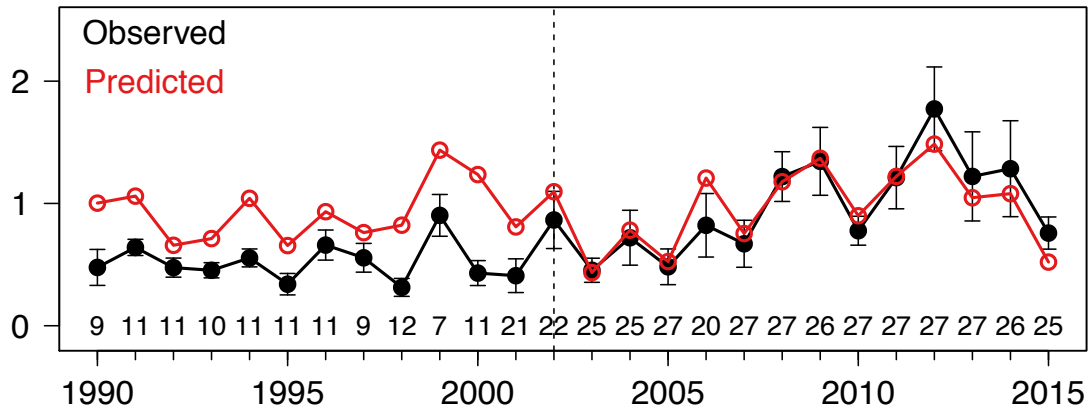


Figure S11. (a) 1990-2015 time series of observed (black) and modeled (red) March monthly mean fine dust concentrations averaged over sites in the Pacific Southwest domain (33° - 39.5° N, 115.5° - 121° W). Error bars denote one standard deviation of the observed means. Predicted values are calculated using a multiple linear regression model with meteorological variables and standard climate indices as predictors, using observed data from 2002 to 2015. The correlation coefficient between 1990-2001 observed and predicted values is 0.56 ($p = 0.07$). The numbers inset show the number of IMPROVE sites used to calculate the regional mean for a given year. (b) 1990-2015 time series of the two variables selected by the regression method: March Standardized Meridional Gradient Index (SMGI, green) of the 500 mb geopotential heights; and March regional relative humidity (RH, blue) averaged over the Pacific Southwest domain. The left axis corresponds to SMGI values (unitless) and the right axis corresponds to RH values (%).

(a) Central SW March fine dust time series ($\mu\text{g m}^{-3}$)



(b) JFM PDO, March SPEI03 and March SMGI time series

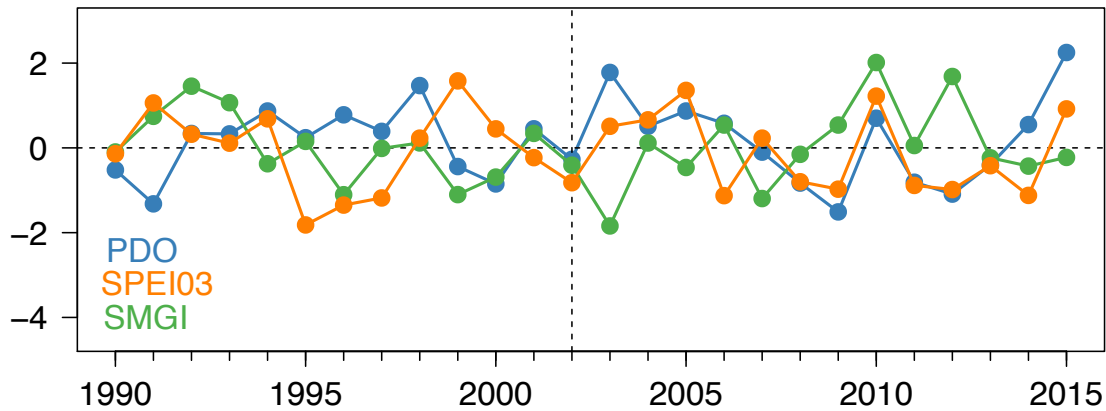


Figure S12. (a) 1990-2015 time series of observed (black) and modeled (red) March monthly mean fine dust concentrations averaged over sites in the Central Southwest domain (33° - 39.5° N, 103° - 115° W). Error bars denote one standard deviation of the observed means. Predicted values are calculated using a multiple linear regression model with meteorological variables and standard climate indices as predictors, using observed data from 2002 to 2015. The correlation coefficient between 1990-2001 observed and predicted values is 0.68 ($p < 0.05$). The numbers inset show the number of IMPROVE sites used to calculate the regional mean for a given year. (b) 1990-2015 time series of the three variables selected by the regression method: JFM Pacific Decadal Oscillation (PDO, blue); March 3-month Standardized Precipitation-Evapotranspiration Index (SPEI03, orange); and March Standardized Meridional Gradient Index (SMGI, green) of the 500 mb geopotential heights.

Table S1. Summary of meteorological variables and standard climate indices considered in our correlation analysis. The meteorological year definition (Dec-Nov) is used.

	Parameter	Units	Data source	Data resolution	Timeframes considered
Meteorological variables ^a	Total precipitation (rain + snow)	inches	PRISM ^b Climate Group	Monthly, 4 km x 4 km regidded to 0.2° x 0.2°, contiguous U.S.	Current month, previous-year JJA and SON, current-year JFM, FMA, or MAM ^f
	Maximum surface air temperature (T_{\max})	°C			
	Mean surface air temperature (T_{mean})	°C			
	Sea surface temperature (SST)	°C	NOAA ERSST V4 ^c	Monthly, 2° x 2° global	
	Sea level pressure (SLP)	mb	NCEP- DOE ^d	Monthly, 2.5° x 2.5°	
	Geopotential height (gph)	m	Reanalysis-II	global	
	Relative humidity (RH)	%			
	Zonal wind	m s ⁻¹	NCEP- DOE ^d Reanalysis-II and MERRA-2 Reanalysis	Monthly, 2.5° x 2.5° (NCEP- DOE) and 0.5° x 0.625° (MERRA-2) global	
	Meridional wind	m s ⁻¹			
	Standardized Precipitation-Evapotranspiration Index (SPEI)	unitless	Spanish National Research Council	Monthly, 0.5° x 0.5° global	1, 3, 6, 12, and 48 months
Standard climate indices	El Niño-Southern Oscillation (ENSO) Oceanic Niño Index (ONI)	°C	NOAA CPC ^e	3-month running mean	3-month running averages from previous-year to current-year JFM, FMA, or MAM ^f
	Pacific Decadal Oscillation (PDO)	unitless		Monthly	
	Western Pacific (WP)	unitless	NOAA CPC ^e	Monthly	Current month and 3- month running averages from previous-year to current-year JFM, FMA, or MAM ^f
	Pacific North American (PNA)	unitless			

^a Data at 1000, 750, 500, and 250 mb pressure levels are considered for geopotential height, meridional and zonal winds, and relative humidity. Other variables are surface data.

^b Parameter-elevation Regression on Independent Slopes Model.

^c National Oceanic and Atmospheric Administration Extended Reconstructed Sea Surface Temperature version 4.

^d National Centers for Environmental Predictions-Department of Energy.

^e National Oceanic and Atmospheric Administration Climate Prediction Center.

^f 3-month average from preceding two months and same month based on the monthly-mean dust values being considered – i.e., JFM for March, FMA for April, and MAM for May dust.